Photodissociation Dynamics of CH₂OO on Multiple Potential Energy Surfaces: Experiment and Theory

Vincent J. Esposito¹, Tianlin Liu^{1,+}, Guanghan Wang^{1,+}, Adriana Caracciolo¹, Michael F. Vansco^{1,†}, Barbara Marchetti², Tolga N. V. Karsili^{2*}, and Marsha I. Lester^{1*}

Department of Chemistry, University of Pennsylvania, Philadelphia, PA 19104-6323 USA
Department of Chemistry, University of Louisiana at Lafayette, Lafayette, LA 70504 USA
Current address: Chemical Sciences and Engineering Division, Argonne National Laboratory, Lemont, IL 60439, USA.

<u>Abstract</u>

UV excitation of the CH₂OO Criegee intermediate across most of the broad span of the (B ¹A') – (X ¹A') spectrum results in prompt dissociation to two energetically accessible asymptotes: O (¹D) + $H_2CO(X^1A_1)$ and $O(^3P) + H_2CO(a^3A'')$. Dissociation proceeds on multiple singlet potential energy surfaces that are coupled by two regions of conical intersection (CoIn). Velocity map imaging (VMI) studies reveal a bimodal total kinetic energy (TKER) distribution for the O (1 D) + H₂CO (X 1 A₁) products with the major and minor components accounting for ca. 40% and ca. 20% on average of the available energy (E_{avl}), respectively. The unexpected low TKER component corresponds to highly internally excited H₂CO (X ¹A₁) products accommodating ca. 80% of E_{avl}. Full dimensional trajectory calculations suggest that the bimodal TKER distribution of the O (1 D) + H₂CO (X 1 A₁) products originates from two different dynamical pathways: a primary pathway (69%) evolving through one CoIn region to products and a smaller component (20%) sampling both CoIn regions enroute to products. Those that access both CoIn regions likely give rise to the more highly internally excited H₂CO (X ¹A₁) products. The remaining trajectories (11%) dissociate to O (³P) + H₂CO (a ³A") products after traversing through both CoIn regions. The complementary experimental and theoretical investigation provides insight on the photodissociation of CH₂OO via multiple dissociation pathways through two regions of CoIn that control the branching and energy distributions of products.

⁺ Equal contributions.

^{*} Corresponding author emails: tolga.karsili@louisiana.edu and milester@sas.upenn.edu

1. Introduction

Criegee intermediates are carbonyl oxide species (RR'C=O⁺O⁻) with zwitterionic character in their ground electronic state, which are produced via alkene ozonolysis reactions in the troposphere.¹ The nascent Criegee intermediates are highly internally excited and can undergo prompt unimolecular decomposition or collisional stabilization. The thermalized Criegee intermediate can then undergo unimolecular decay or bimolecular reaction with trace atmospheric species (primarily water vapor, SO₂, and organic acids).² Recent laboratory generation of Criegee intermediates via alternative synthetic schemes have enabled spectroscopic, kinetic, and dynamical studides of these fascinating chemical species.^{3–5}

The simplest Criegee intermediate CH₂OO has been widely investigated using ultraviolet (UV) spectroscopy. Laboratory studies revealed a strongly absorbing electronic excited state accessed via a π^* $\leftarrow \pi$ transition centered on the carbonyl oxide moiety.⁶⁻⁹ CH₂OO exhibits a broad UV spectrum spanning from 280 to 450 nm (FWHM \geq 40 nm), which peaks at \sim 340 nm ($\sigma_{abs} \sim 10^{-17}$ cm²).⁷ The strong UV absorption provides a sensitive way to detect CH₂OO and has been utilized extensively to investigate its bimolecular reactions with key atmospheric species. Nevertheless, questions remain on the photochemistry of CH₂OO upon UV excitation, which are addressed in this work utilizing a combination of experimental and theoretical approaches.

The UV absorption spectrum of CH₂OO has also been characterized theoretically. Specifically, Dawes et al. ¹⁰ computed CH₂OO potential energy profiles along the O-O stretch coordinate in the ground X ¹A' and optically bright B ¹A' electronic states, hereafter denoted as the S₀ and S₂ states, respectively, using the explicitly correlated multireference configuration interaction (MRCI-F12) method and obtained the UV absorption spectrum of CH₂OO, which accurately reproduced the experimental spectrum. ⁶⁻⁸ In addition, this and an earlier study ¹¹ examined the low-lying singlet states along the O-O dissociation coordinate, revealing two regions of conical intersection (CoIn) that play a key role in the dissociation dynamics. CoIn are degeneracies between distinct electronic states of the same spin multiplicity. They are integral parts of multi-dimensional potential energy surfaces and are implicated in many ultrafast phenomena observed in molecular photochemistry. ^{12,13}

UV excitation of CH₂OO to the S₂ state leads to rapid dissociation, forming O (1 D) + H₂CO (X 1 A₁) and O (3 P) + H₂CO (a 3 A") products, as revealed by previous photodissociation studies in this laboratory. An upper limit for the threshold of the higher energy O (3 P) + H₂CO (a 3 A") products channel was determined to be $\leq 75.7 \pm 0.3$ kcal mol $^{-1}$. Using the known energy splittings between the singlet and triplet O-atoms and H₂CO, the dissociation energy of CH₂OO to O (1 D) + H₂CO (X 1 A₁) products was determined to be $\leq 49.0 \pm 0.3$ kcal mol $^{-1}$, in good agreement with theoretical

predictions. 10,14,16,19,20 This indicates that dissociation to O (1 D) + H₂CO (X 1 A₁) products is energetically feasible across the entire UV absorption spectrum of CH₂OO, while dissociation to the higher energy O (3 P) + H₂CO (a 3 A") product channel is only possible at $\lambda \leq 378$ nm. In addition, the O (1 D) action spectrum of CH₂OO follows the profile of the UV absorption spectrum of CH₂OO, 6 while the O (3 P) action spectrum peaks at shorter wavelength (ca. 330 nm) and tails off rapidly on the long-wavelength edge. 15

An early theoretical study reported that the excited S_2 state is dissociative with respect to the O-O coordinate and predicted that CH_2OO forms $O(^1D) + H_2CO(X^1A_1)$ products upon electronic excitation to the S_2 state. 11 More recently, a full dimensional (9D) quantum dynamics study by Meng and Meyer 21 investigated the $CH_2OO(B^1A')$ state dissociation utilizing a multilayer multiconfigurational time-dependent Hartree approach based on a high level MRCI reference. This study focused exclusively on the dissociation dynamics to $O(^1D) + H_2CO(X^1A_1)$ products. Another recent theoretical study characterized the singlet state-mediated dissociation products and their branching ratios following $CH_2OO(S_2 \leftarrow S_0)$ excitation. In this work, Samanta et al. 22 used a dynamically-weighted complete active space self-consistent field method (DW-CASSCF) with quantum dynamics propagated on a two-dimensional (2D) potential energy surface (OO distance and COO angle). This reduced dimensional calculation predicted that the $O(^3P) + H_2CO((a^3A''))$ product channel increases above the dissociation threshold and ultimately becomes the dominant product channel. As noted by Dawes et al., 10 the excited state potentials utilized in the dynamical studies by Meng and Meyer and Samanata et al. 22 do not provide a good representation in the Franck-Condon region.

The present study presents a joint experimental and computational investigation of the UV photodissociation dynamics of CH_2OO leading to $O(^1D) + H_2CO(X ^1A_1)$ and $O(^3P) + H_2CO(a ^3A'')$ products. The experiments utilize velocity map imaging (VMI) to obtain the kinetic energy release to products in both channels. A combination of quantum chemistry and trajectory surface hopping approaches is used to map the singlet potentials and follow the rapid evolution of CH_2OO from the excited S_2 state to products through multiple pathways. This combined experimental and theoretical study provides new insights on the photochemistry of CH_2OO , including energy dissipation and branching to products.

2. Methods

2.1 Experimental

The simplest Criegee intermediate, CH₂OO, is generated by photolysis of CH₂I₂ and subsequent reaction of the CH₂I radical with O₂.³ In this laboratory, CH₂I₂ vapor is entrained in a 10% O₂/Ar carrier gas and pulsed from a solenoid valve through a quartz capillary tube reactor, where it is photolyzed using a KrF excimer laser at 248 nm. The resultant CH₂OO is collisionally stabilized in the capillary and jet-

cooled in the subsequent supersonic expansion. Approximately 4 cm downstream in a collision-free region, the molecular beam is crossed by a UV pump (310 – 350 nm) and UV probe beams generated by Nd: YAG pumped dye lasers. The UV pump excitation results in photodissociation of CH₂OO, producing O (¹D) and/or O (³P) products that are probed after a 50 ns delay. Specifically, a UV probe laser at 205.47 nm ionizes O (¹D) [or 225.66 nm to ionize O (³P)] products by 2+1 resonant-enhanced multiphoton ionization (REMPI).^{23,24} The O⁺ ions are investigated using VMI to obtain the angular and total kinetic energy release (TKER) distributions resulting from UV photodissociation of CH₂OO. Further experimental details are described in the Supporting Information (SI).

2.2 Theoretical

The equilibrium geometry, harmonic frequencies, and normal mode wavenumbers of CH₂OO were obtained at the ω-B97X-D/6-31G(*d*) level of theory. ^{25–27} Following this, a 1-dimensional (1D) cut of the adiabatic potential energy (PE) surface along the O-O bond coordinate was calculated using the complete active space 2nd order perturbation theory (CASPT2) method^{28–30} in conjunction with Dunning's augmented double-ζ basis set, aug-cc-pVDZ, ³¹ holding all other coordinates fixed at their ground state equilibrium values. The CASPT2 calculations were based on a 7-singlet state-averaged complete active space self-consistent field^{32,33} (SA7-CASSCF) reference wavefunction employing an active space of 10 electrons in 8 orbitals. These orbitals are depicted in Figure S1 of the SI.

Trajectory surface hopping (TSH) simulations were performed using the molecular dynamics with quantum transitions surface hopping method devised by Hammes-Schiffer and Tully³⁴ and implemented in Newton-X.^{35,36} The initial positions and momenta of the ground state were obtained via a Wigner distribution based on the harmonic frequencies of the global minimum of the ground state calculated at the ω-B97X-D/6-31G(*d*) level of theory. In the TSH simulations, the nuclear coordinates were propagated by integrating Newton's equation using the velocity Verlet method, ^{37,38} while the electronic coordinates were propagated by numerically solving the time-dependent Schrödinger equation using Butcher's fifth-order Runge-Kutta method in steps of 0.005 fs.³⁹ Trajectories were initiated on the S₂ state and the associated energies and gradients of the lowest singlet electronic states were computed 'on-the-fly' using the CASSCF(10/8)/aug-cc-pVDZ level of theory via the COLUMBUS^{40,41} interface⁴² to Newton-X. In order to evaluate the hopping probability, nonadiabatic couplings were computed by evaluating the non-adiabatic coupling matrix elements derived from the CASSCF computations. 120 trajectories were propagated in time with a step size of 0.5 fs for a maximum propagation time of 50 fs. The CASSCF and CASPT2 calculations are carried out using MOLPRO⁴³ while the DFT calculations are performed in Gaussian 09.⁴⁴

3. Results and Discussion

3.1 Potential Energy Profiles

The ground state minimum energy geometry of CH_2OO is planar with the terminal oxygen pointed towards one of the hydrogens. Vertical excitation to the S_1 state involves an $\pi^* \leftarrow$ n transition and has no oscillator strength, while excitation to the S_2 state is a strong $\pi^* \leftarrow \pi$ transition with an oscillator strength of 0.095 (see orbital diagram in Figure S1). As a result, electronic excitation of CH_2OO is expected to populate the bright S_2 state exclusively.

Since previous theoretical and experimental studies have indicated the importance of O-O bond dissociation upon UV excitation, 1-D adiabatic PE profiles of the lowest 7 singlet electronic states were calculated along the O-O bond stretch coordinate (R_{OO}) using CASPT2(10,8)/aug-cc-pVDZ and CASSCF(10,8)/aug-cc-pVDZ methods, and are shown in Figure 1. Since these PE profiles are unrelaxed rigid-body scans, the asymptotic limits represent upper limits to the true dissociation energies. In the current model, the H_2CO fragments at long R_{OO} are best described as internally excited. These types of rigid-body scans are a reasonable approximation since the prompt O-O bond fission on a repulsive PE surface occurs on a timescale that is much shorter than intramolecular vibrational relaxation. The change in chemical bonding between the zwitterionic $H_2C=O^+O^-$ Criegee intermediate and the singlet and triplet formaldehde $H_2C=O$ products indicates that the CO bond length and other coordinates change significantly upon dissociation as discussed below, leading to highly internally excited H_2CO products.

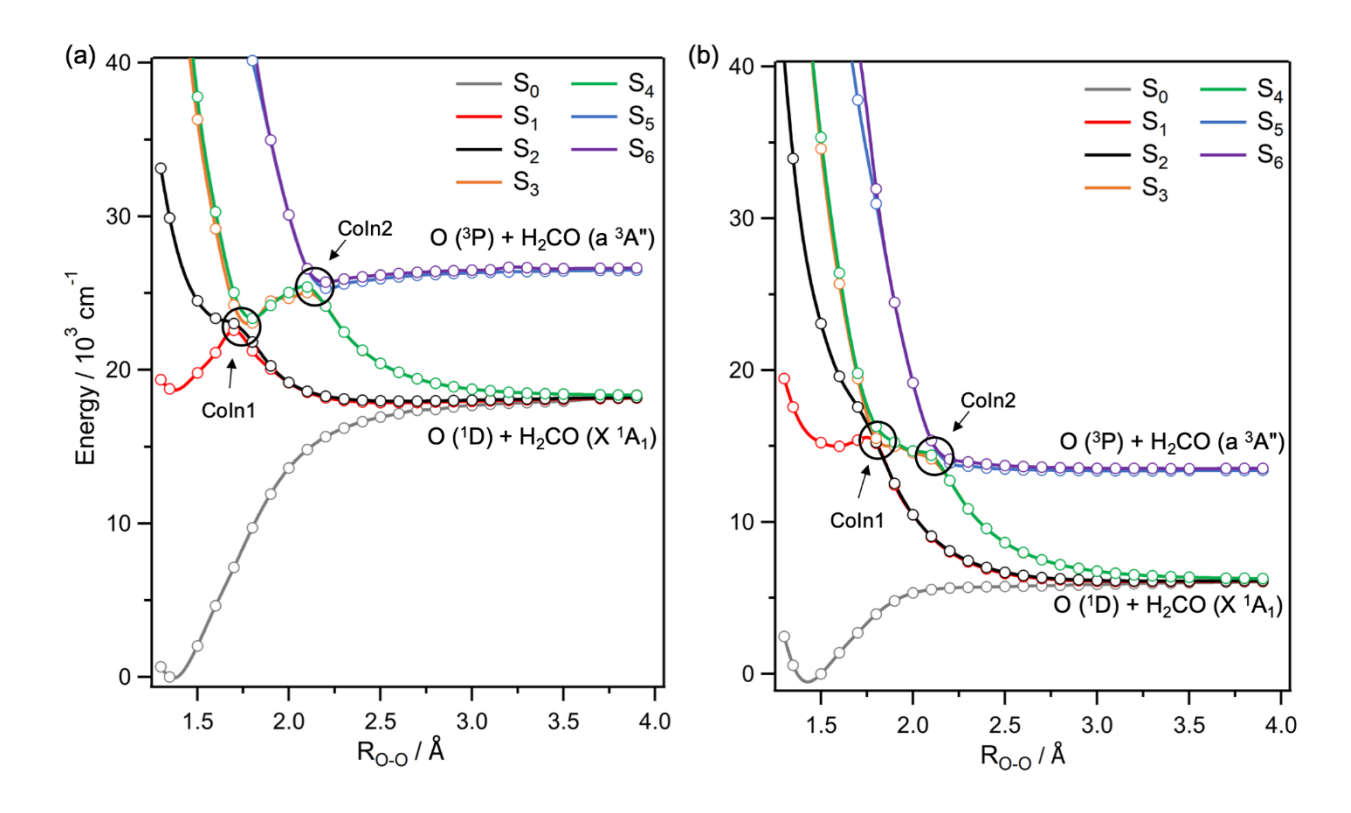


Figure 1. (a) CASPT2(10,8)/aug-cc-pVDZ and (b) CASSCF(10,8)/aug-cc-pVDZ potential energy surfaces for the 7 lowest lying singlet electronic states of CH₂OO along the O-O bond coordinate. All other coordinates held fixed at equilibrium geometry.

The ground state of CH_2OO (S_0) is bound and correlates adiabatically to the lowest energy asymptote that forms $O(^1D) + H_2CO$ (X^1A_1) products as shown in Figure 1. The S_1 and S_2 states are quasi-bound, adiabatically correlating with the lowest energy asymptote at long R_{OO} and diabatically correlating with the first electronically-excited asymptote that forms $O(^3P) + H_2CO$ (a^3A'') products. At $R_{OO} \sim 1.7$ Å, the S_1 and S_2 states encounter an avoided crossing with the S_3 and S_4 states, which develops into a conical intersection (CoIn1) when orthogonal motions are considered. A further avoided crossing is observed at $R_{OO} \sim 2.1$ Å, again developing into a conical intersection (CoIn2), that involves the S_3 , S_4 , S_5 and S_6 states. These two regions of conical intersection are unusual due to the apparent presence of 4 interacting states (or two 2-state intersections that are close in configuration space) in the region of each CoIn, whereas many photochemical processes result from CoIn with 2 or 3 interacting states. Both CoIns are expected to play a role in the product branching to the two asymptotic product limits discussed above.

Following excitation to S_2 , the population can traverse the region around CoIn1, continuing along the adiabatic S_2 to form the lowest energy asymptotic products, or passing through CoIn1 and undergoing internal conversion to the higher energy S_3 or S_4 states. If the latter prevails, the evolving S_3 or S_4 population will encounter CoIn2. Again, traversing around or through CoIn2 will lead to the ground and first-excited asymptotic products, respectively. In order to form the higher-energy $O(^3P) + H_2CO$ (a $^3A''$) products, internal conversion occurs from a lower-energy state to a higher-energy state at two separate CoIn locations. Note that two different pathways lead to $O(^1D) + H_2CO$ (X^1A_1) products: (1) passage around CoIn1 and continuing along S_2 to products or (2) passing through CoIn1 to the region of CoIn2 and evolving along S_3 or S_4 to the same products.

3.2 Velocity Map Imaging Studies

Prior experimental VMI studies of the UV photodissociation dynamics of CH₂OO with detection of O (1 D) products focused on excitation at $\lambda > 360$ nm where the lowest spin-allowed channel to O (1 D) + H₂CO (X 1 A₁) products is the only or the predominant product channel energetically available. 16 UV excitation of CH₂OO from 364 to 417 nm results in TKER distributions that are broad and unstructured. In the prior report, 16 the TKER distributions were fit using a polynomial function to extract the peak and breadth of the distributions. Here, the data is reanalyzed using a single Gaussian function to extract the average and breadth of the TKER distributions (Table S1; 380 nm data also included in Table 1), which gives analogous results. Both analyses yield average TKER ranging from 4100 to 3200 cm⁻¹ that accounts for ca. 40-50% of the available energy ($E_{av1} \sim 7000-10,000$ cm⁻¹, derived from photon energy

minus the dissociation energy to O (1 D) + H_{2} CO ($X^{1}A_{1}$) products. The initial internal energy of supersonic jet-cooled CH₂OO is assumed to be negligible). This indicates that corresponding internal (vibrational and/or rotational) excitation of the H_{2} CO ($X^{1}A_{1}$) product accommodates 50-60% of E_{avl} .

The high degree of vibrational excitation of the H₂CO (X ¹A₁) fragment can be understood by the significant changes in the geometric structure and associated vibrational frequencies for H₂CO (X ¹A₁) products compared to CH₂OO (X ¹A') (Figure 2, Table S3). Specifically, we anticipate extensive vibrational excitation of the CO stretch and CH₂ wag of the H₂CO (X ¹A₁) products arising from ca. 20% and 24% increases in these vibrational frequencies, respectively.

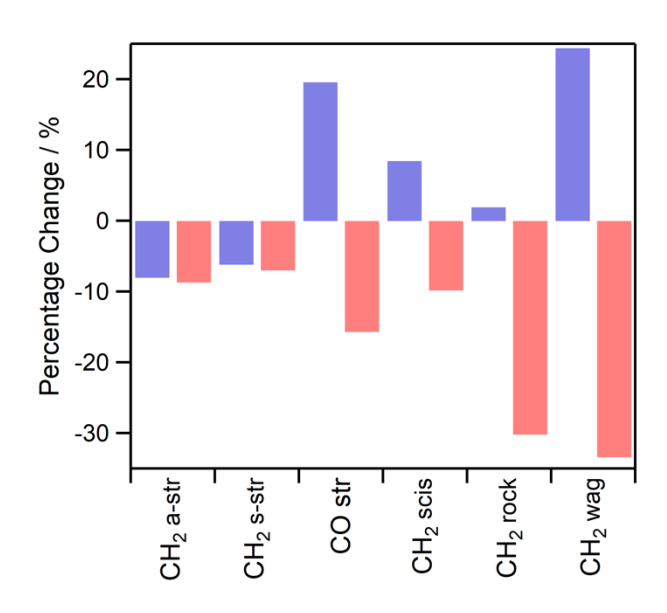


Figure 2. The vibrational modes with the most significant changes (%) in frequency between $CH_2OO(X^1A')$ and $H_2CO(X^1A_1)$ (blue bars) or $H_2CO(a^3A'')$ (red bars) products.

Smaller (\leq 10%) changes in vibrational frequencies are predicted for the symmetric and asymmetric CH stretches (decrease) and CH₂ scissor mode (increase). In addition, we note that a simple impulsive model⁴⁵ suggests that rotation of the H₂CO (X 1 A₁) products will accommodate ca. 23% of the average translational energy ($E_{rot} \sim$ ca. 1000 cm⁻¹).¹⁴ Overall, the TKER distributions lack structure because of the high degree of internal excitation of the H₂CO (X 1 A₁) products.

For UV excitation of CH₂OO at $\lambda = 330$ and 350 nm, a prior study utilized VMI detection of the O (³P) products to examine the TKER release to the higher-energy spin-allowed dissociation channel that yields O (³P) + H₂CO (a ³A") products. ¹⁵ Again, reanalysis of experimental TKER data shown in Figure 3 (red) yields single Gaussian distributions with similar average (Table 1) and breadth (Table S1) for each

of the TKER distributions as that previously reported using polynomial fits. Specifically, the average of the TKER distribution accounts for 40-50% of the available energy ($E_{avl} \sim 2000\text{-}4000 \text{ cm}^{-1}$, derived from photon energy minus the dissociation energy to O (3P) + H₂CO (a $^3A''$) products). As a result, internal excitation of the H₂CO (a $^3A''$) product accommodates the remaining 50-60% of the available energy.

Similarly, vibrational excitation of the triplet H_2CO (a $^3A''$) products can be rationalized based on the geometric structure and associated vibrational frequency changes between CH_2OO and H_2CO (a $^3A''$) products (Figure 2, Table S3). Here, we expect vibrational excitation of the CH_2 group arising from ca. 30% reduction in the frequencies of CH_2 wag and CH_2 rock modes of the H_2CO (a $^3A''$) products. In addition, there is a ca. 16% reduction in the CO stretch frequency, which will result in CO stretch excitation of the H_2CO (a $^3A''$) products. Smaller ($\leq 10\%$) decreases are also predicted in the frequencies of the symmetric and asymmetric CH stretches and CH_2 scissor modes. A limited degree of rotational excitation ($E_{rot} \sim ca. 400 \text{ cm}^{-1}$) is anticipated based on the impulsive model.

In the current work, we utilize VMI to examine O (1 D) products following photodissociation of CH₂OO at UV excitation from 310 to 350 nm, where both the O (1 D) + H₂CO (X 1 A₁) and O (3 P) + H₂CO (a 3 A") product channels are open and energetically accessible. These experiments reveal a surprising result: the TKER distributions exhibit bimodal distributions as shown in Figure 3 (and Figure S2). The TKER distributions are well-represented by a bimodal Gaussian-Gumbel function with the low TKER component fit as a Gumbel distribution (Tables 1 and S2). The main TKER component is broad and structureless with average TKER of 4700 to 6600 cm⁻¹, accounting for 41-44% of the available energy ($E_{av1} \sim 11,000$ to 15,000 cm⁻¹, derived from photon energy minus the dissociation energy to O (1 D) + H₂CO (X 1 A₁) products). This is similar product energy partitioning as observed upon UV excitation of CH₂OO at $\lambda > 360$ nm (Table S1).

Surprisingly, however, we observe that the TKER distributions obtained with O (1 D) detection upon UV excitation of CH₂OO from 310 to 350 nm have an additional low TKER component with average energy of 2000 to 3800 cm⁻¹ (Tables 1 and S1) that corresponds to 16-25% of the available energy ($E_{avl} \sim 11,000$ to 15,000 cm⁻¹). Representative experimental TKER distributions obtained at 330 and 350 nm are shown in Figure 3 (blue); additional results are shown in Figure S2. This low TKER component accounts for 10-23% of the O (1 D) product yield. The corresponding average internal excitation of the H_2 CO (X 1 A₁) products is 9000 to 11,500 cm⁻¹ or a remarkable 75 to 84% of the available energy. As the trajectory calculations that follow will show, these highly internally excited H_2 CO (X 1 A₁) products arise from frustrated dissociation events. Following UV excitation of CH₂OO, some of the separating products heading toward the O (3 P) + H_2 CO (3 A") asymptote are rerouted in the vicinity of a conical intersection (CoIn2) and emerge as highly internally excited H_2 CO (X 1 A₁) + O (1 D) products.

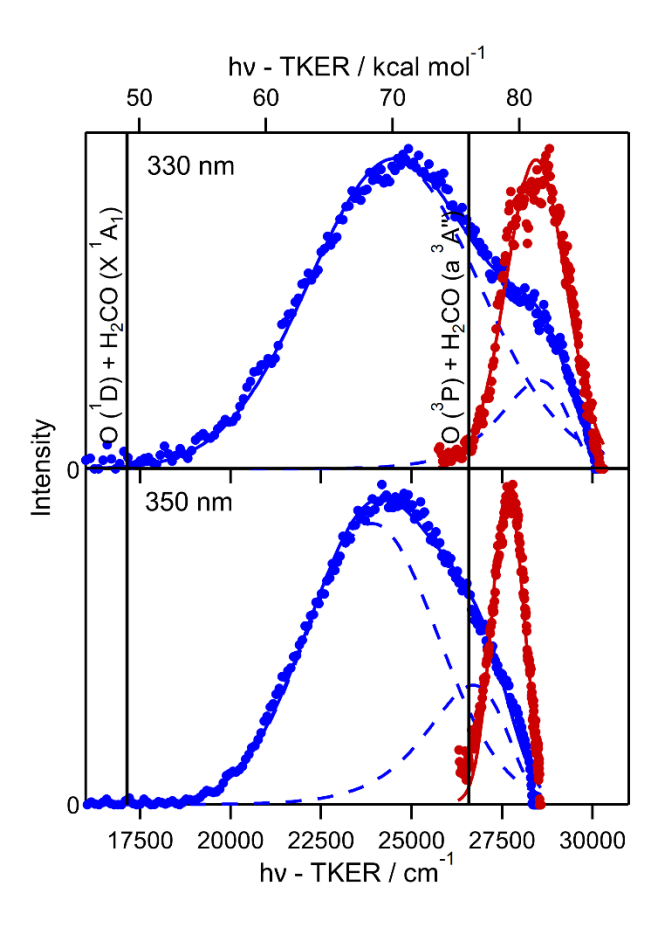


Figure 3. VMI investigation of the O (1 D) products following UV excitation of CH₂OO at 330 nm and 350 nm yields total kinetic energy release (TKER) distributions for the O (1 D) + H₂CO (X 1 A₁) products (blue points). A bimodal Gaussian-Gumbel fit to the TKER distribution (solid) and the individual components (dashed) are shown, where the low TKER component is fit as a Gumbel distribution. A prior VMI study of the O (3 P) products following UV excitation of CH₂OO at 330 and 350 nm yielded the TKER distributions for the O (3 P) + H₂CO (a 3 A") products (red points, adapted from Li, H.; Fang, Y.; Beames, J. M.; Lester, M. I. *J. Chem. Phys.* **2015**, *142*, 214312, with permission of AIP Publishing) with Gaussian fits (solid). The TKER distributions are plotted relative to photon energy (h ν – TKER). The peak amplitudes of the two product channels are set equal (normalized). The vertical lines indicate the O (1 D) + H₂CO (X 1 A₁) (49.0 ± 0.3 kcal mol⁻¹) and O (3 P) + H₂CO (a 3 A") (75.7 ± 0.3 kcal mol⁻¹) dissociation limits.

Table 1. Characteristics of the total kinetic energy release (TKER) distributions derived from reconstructed velocity map images of O (¹D) and O (³P) products following UV excitation of CH₂OO.

λ (nm)	$E_{avl} (cm^{-1})$	$\langle \text{TKER} \rangle_{l}$ (cm ⁻¹)	$\frac{E_{\text{int,1}}}{E_{\text{avl}}}(\%)$	$\langle \text{TKER} \rangle_2$ (cm ⁻¹)	$\frac{E_{\text{int,2}}}{E_{\text{avl}}}(\%)$	TKER ₂ contribution (%)
O (¹D) detection						
310^a	15160	6570(120)	57	3830(200)	75	23(3)
320^a	14150	6150(40)	57	2640(60)	81	12(1)
330^a	13200	5800(40)	56	2290(60)	83	11(1)
340^a	12310	5200(40)	58	2000(60)	84	10(1)
350^a	11470	4660(110)	59	2480(130)	78	22(3)
380^b	9220	3810(10)	59	-	-	-
O (³ P) detection						
330 ^c	3830	1870(10)	51	-	-	-
350 ^c	2100	910(10)	57	-	-	-

^a Bimodal Gaussian-Gumbel fit of TKER distribution with low TKER component fit as a Gumbel distribution

3.3 Trajectory Surface Hopping Calculations

In order to interpret the experimental results, trajectory surface hopping (TSH) molecular dynamics simulations are also performed. Given the large active space and number of states, it is computationally expensive to perform the TSH simulations using the preferred CASPT2 method. Instead, we have used CASSCF with the same basis set as the CASPT2 PE profiles, which has been utilized for TSH studies of Criegee intermediates in the past. However, the lack of dynamic correlation in the CASSCF method will manifest in less accurate TSH simulations, which may impact the resultant dynamics and branching ratios. As evident from the CASPT2 and CASSCF PE profiles in Figure 1, the relative CASSCF/CASPT2 energies of the product asymptotes are different (e.g. relative to the Franck-Condon excitation region), although the vertically excited electronic states correlate to the same asymptotic limits as in CASPT2. Additionally, in both cases, the vertically excited S₂ state is above the energetic threshold for forming both ground and first electronically excited asymptote limits. The following discussion of the trajectories is intended to provide a qualitative description of the dissociation dynamics and illustrate that population evolves to both asymptotes with branching at both CoIn1 and CoIn2.

^b Reanalysis of TKER distribution derived from O (¹D) products in Ref. 16 with a Gaussian fit.

^c Reanalysis of TKER distributions derived from O (³P) products in Ref. 15 with a Gaussian fit.

The TSH simulations show prompt O-O bond dissociation within 40 fs following vertical excitation to the S_2 state. Figure 4 shows trajectory probability amplitude as a function of time for the 7 lowest-energy singlet states of CH₂OO. Trajectories are initiated on the S_2 state and many undergo rapid conversion to S_1 and S_0 . As time evolves, a portion of the amplitude distributes across all 7 singlet states. The trajectories end with the S_0 , S_1 , S_2 , S_3 , and S_4 states leading to O (1 D) + H₂CO (X 1 A₁) products having significantly greater amplitude than the higher S_5 and S_6 states that form O (3 P) + H₂CO (a 3 A") products. The dominant electronic configurations of the products are confirmed by visualizing the CASSCF molecular orbitals at the final time-step. Representative analysis is shown in Figure S3.

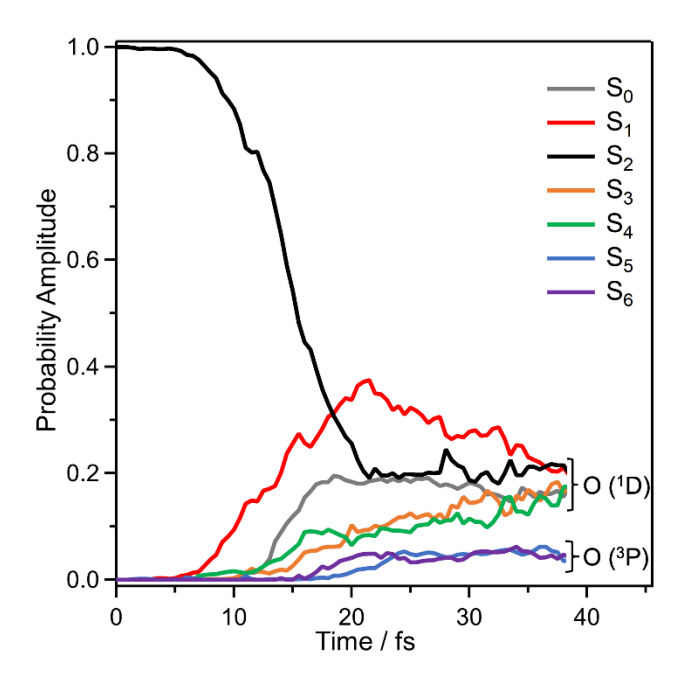


Figure 4. Probability amplitude in time evolution (fs) of CH₂OO along multiple dissociative potentials leading to O (1 D) + H₂CO (X 1 A₁) and O (3 P) + H₂CO (a 3 A") products. CH₂OO is initially prepared in the S₂ state (black) via a $\pi^* \leftarrow \pi$ electronic excitation.

Representative trajectories for three distinct O-O dissociation pathways initiated on S_2 are shown in Figure 5. The primary dissociation pathway (69%) corresponds to direct dissociation via CoIn1 to form O (1 D) + H₂CO (X 1 A₁) products as shown in panel (a). This trajectory starts with internal conversion from S_2 to the lower S_1 state near the region of CoIn1 and continues to form O (1 D) + H₂CO (X 1 A₁) products. The remaining 31% of the trajectories undergo internal conversion to a higher state (e.g. S_3 or S_4) at CoIn1 and are directed toward CoIn2. In the vicinity of CoIn2, 20% of the trajectories follow the adiabatic path around CoIn2 and form O (1 D) + H₂CO (X 1 A₁) products as illustrated in panel

(b). The remaining 11% traverse the non-adiabatic path through CoIn2 and form O (3 P) + H₂CO (a 3 A") products as shown in panel (c).

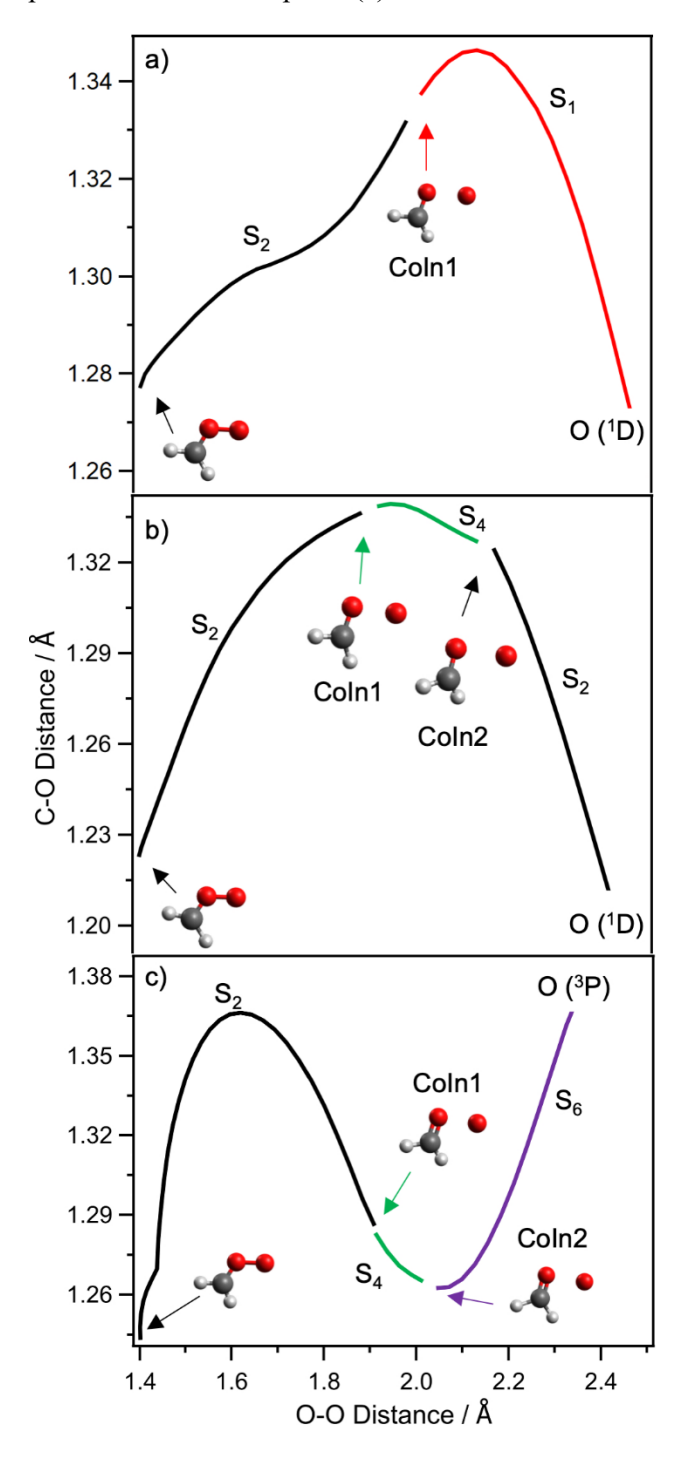


Figure 5. Representative surface hopping trajectories illustrating three dynamical pathways for dissociation following electronic excitation of CH₂OO to the S₂ state (black). (a) Trajectory follows S₂ to CoIn1 region, where it couples to S₁ (red) and dissociates along O-O coordinate to O (1 D) + H₂CO (X 1 A₁) products. (b) Trajectory follows S₂ to CoIn1 region, where it couples to S₄ (green). Near CoIn2, the trajectory switches back to S₂ and dissociates to O (1 D) + H₂CO (X 1 A₁) products. (c) Trajectory follows

 S_2 to CoIn1 region, again switching to S_4 state and then switching to S_6 (purple) in CoIn2 region. Dissociation along S_6 leads to O (3P) + H_2CO (a $^3A''$) products. Note that displacement along the C-O coordinate represents C-O vibrational excitation of the H_2CO product.

The representative trajectories in panels (a) and (b) both produce O (1 D) + H₂CO (X 1 A₁) products but via different pathways. These two distinct pathways are expected to yield different internal energy distributions for the H₂CO (X 1 A₁) products and different corresponding TKER distributions. Trajectories that sample both CoIn1 and CoIn2 regions, e.g. panel (b), are likely to result in more highly internally excited H₂CO (X 1 A₁) products. These types of trajectories are associated with the low TKER component and high internal excitation (75-84% of E_{avl}) that accounts for 10-23% of the O (1 D) + H₂CO (X 1 A₁) products in the experiment.

The partitioning of internal energy of the excited H₂CO (X ¹A₁) products into vibrational and rotational degrees of freedom is captured in the trajectory calculations. As discussed previously, extensive excitation in CO stretch is expected during dissociation due to the large geometrical changes between CH₂OO and singlet or triplet H₂CO products. This excitation can be seen in each trajectory (Figure 5) as oscillations in the C-O distance. For example, in panel (c) a full period of the CO stretch motion occurs, consistent with vibrational excitation of the H₂CO (a ³A") fragment. Additionally, the change in orientation of CH₂OO from the beginning of each trajectory to products reflects rotational excitation of the H₂CO fragment initiated by the recoil imparted in O-O bond breakage.

A previous theoretical study examined the branching between O (1 D) + H₂CO (X 1 A₁) and O (3 P) + H₂CO (a 3 A") products in the photodissociation of CH₂OO. 22 The earlier two dimensional (O-O stretch and COO bend) quantum dynamics study predicted that non-adiabatic coupling would lead to 5% forming O (1 D) + H₂CO (X 1 A₁) products and the remaining 95% yielding O (3 P) + H₂CO (a 3 A") products. 22 The current full dimensional TSH study suggests strong coupling in both the CO stretch (Figure 5) and the HCOO torsion (Figure S4) in the regions of CoIn along the dissociation coordinate. The lack of obvious activity in the COO bend indicates a small impact of the COO bending coordinate on the internal conversion process at each CoIn. Instead, torsion appears to be an important coupling mode as found in several prototypical photodissociation cases. $^{49-52}$ The primary reason for the prominence of torsion is that it is a symmetry conserving mode that is local to the dissociation coordinate. Prior experiments using UV action spectroscopy with detection of O (1 D) and O (3 P) products, and related modeling, also indicate that O (1 D) + H₂CO (X 1 A₁) is the primary product channel and O (3 P) + H₂CO (a 3 A") is a minor channel at UV excitation energies where both are open, 15 consistent with the present trajectory calculations.

4. Conclusions

The photodissociation dynamics of the CH₂OO Criegee intermediate is probed experimentally and theoretically following UV excitation to the S₂ state on the strong $\pi^* \leftarrow \pi$ transition. Dissociation

leads to two product asymptotes: $O(^1D) + H_2CO(X ^1A_1)$ and $O(^3P) + H_2CO(a ^3A'')$. This study examines the role of the two CoIns that couple the lowest 7 singlet PE surfaces of CH_2OO in determining the dissociation pathways, energy dissipation, and branching between the products channels. Future studies are planned to reexamine the dynamics at a higher level of electronic structure theory.

VMI experiments reveal bimodal TKER distributions for O (1 D) + H₂CO (X 1 A₁) products upon UV excitation at 310-350 nm, where both product channels are open. The primary TKER component accounts for ca. 40% of E_{avl}, which is similar to the TKER distribution obtained when only the O (1 D) + H₂CO (X 1 A₁) channel is energetically accessible (λ > 360 nm). In addition, a surprising low TKER component (ca. 10-23% contribution) accommodating less than 25% of E_{avl} is also identified, which corresponds to highly internally excited H₂CO (X 1 A₁) products with 75-84% of E_{avl}. The VMI distribution obtained for O (3 P) + H₂CO (a 3 A") products show TKER distributions accounting for 40-50% of E_{avl}.

Complementary trajectory calculations reveal two dynamical pathways leading to O (1 D) + H₂CO (X 1 A₁) products. Both begin with evolution along S₂ to CoIn1 and then either (a) continue to dissociation (69%) or (b) couple with S₃ or S₄ to access the CoIn2 region before dissociation (20%). Pathway (a) leads to moderate internal excitation of H₂CO (X 1 A₁), while pathway (b) is expected to result in highly internally excited H₂CO (X 1 A₁) products. Together, these two dynamical pathways are consistent with the bimodal TKER distribution for O (1 D) + H₂CO (X 1 A₁) products observed experimentally. The remaining 11% of trajectories evolve through CoIn2 to form O (3 P) + H₂CO (a 3 A") products. Together, experimental and theoretical studies of the photodissociation of CH₂OO reveal distinct dynamical pathways through regions of conical intersection that control the outcome.

Supplementary Information

Expanded description of experimental methods and velocity map imaging data. Molecular orbitals describing relevant electronic transitions, theoretical geometry and frequency data, and additional trajectory data.

Acknowledgments

The experimental research at the University of Pennsylvania is primarily supported through the U.S. Department of Energy-Basic Energy Sciences under grant DE-FG02-87ER13792. The theoretical research is partially supported by a National Science Foundation Graduate Research Fellowship Program under Grant No. DGE-1845298 (VJE) and by the National Science Foundation under Grant agreement CHE-2003422 (TNVK).

References

- (1) Johnson, D.; Marston, G. The Gas-Phase Ozonolysis of Unsaturated Volatile Organic Compounds in the Troposphere. *Chem. Soc. Rev.* **2008**, *37*, 699–716.
- (2) Chhantyal-Pun, R.; Khan, M. A. H.; Taatjes, C. A.; Percival, C. J.; Orr-Ewing, A. J.; Shallcross, D. E. Criegee Intermediates: Production, Detection and Reactivity. *Int. Rev. Phys. Chem.* **2020**, *39*, 385–424.
- (3) Welz, O.; Savee, J. D.; Osborn, D. L.; Vasu, S. S.; Percival, C. J.; Shallcross, D. E.; Taatjes, C. A. Direct Kinetic Measurements of Criegee Intermediate (CH₂OO) Formed by Reaction of CH₂I with O₂. *Science* **2012**, *335*, 204–207.
- (4) Taatjes, C. A.; Shallcross, D. E.; Percival, C. J. Research Frontiers in the Chemistry of Criegee Intermediates and Tropospheric Ozonolysis. *Phys. Chem. Chem. Phys.* **2014**, *16*, 1704–1718.
- (5) Osborn, D. L.; Taatjes, C. A. The Physical Chemistry of Criegee Intermediates in the Gas Phase. *Int. Rev. Phys. Chem.* **2015**, *34*, 309–360.
- (6) Beames, J. M.; Liu, F.; Lu, L.; Lester, M. I. Ultraviolet Spectrum and Photochemistry of the Simplest Criegee Intermediate CH₂OO. *J. Am. Chem. Soc.* **2012**, *134*, 20045–20048.
- (7) Sheps, L. Absolute Ultraviolet Absorption Spectrum of a Criegee Intermediate CH₂OO. *J. Phys. Chem. Lett.* **2013**, *4*, 4201–4205.
- (8) Ting, W.-L.; Chen, Y.-H.; Chao, W.; Smith, M. C.; Lin, J. J.-M. The UV Absorption Spectrum of the Simplest Criegee Intermediate CH₂OO. *Phys. Chem. Chem. Phys.* **2014**, *16*, 10438–10443.
- (9) Foreman, E. S.; Kapnas, K. M.; Jou, Y.; Kalinowski, J.; Feng, D.; Gerber, R. B.; Murray, C. High Resolution Absolute Absorption Cross Sections of the B ¹A'-X ¹A' Transition of the CH₂OO Biradical. *Phys. Chem. Chem. Phys.* **2015**, *17*, 32539–32546.
- (10) Dawes, R.; Jiang, B.; Guo, H. UV Absorption Spectrum and Photodissociation Channels of the Simplest Criegee Intermediate (CH₂OO). *J. Am. Chem. Soc.* **2015**, *137*, 50–53.
- (11) Aplincourt, P.; Henon, E.; Bohr, F.; Ruiz-Lopez, M. F. Theoretical Study of Photochemical Processes Involving Singlet Excited States of Formaldehyde Carbonyl Oxide in the Atmosphere. *Chem. Phys.* **2002**, *285*, 221–231.
- (12) Domcke, W.; Yarkony, D. R.; Köppel, H. *Conical Intersections: Electronic Structure, Dynamics and Spectroscopy*; Advanced Series in Physical Chemistry; World Scientific, 2004; Vol. 15.
- (13) Domcke, W.; Yarkony, D. R.; Köppel, H. *Conical Intersections: Theory, Computation and Experiment*; Advanced Series in Physical Chemistry; World Scientific, 2011; Vol. 17.
- (14) Lehman, J. H.; Li, H.; Beames, J. M.; Lester, M. I. Communication: Ultraviolet Photodissociation Dynamics of the Simplest Criegee Intermediate CH₂OO. *J. Chem. Phys.* **2013**, *139*, 141103.
- (15) Li, H.; Fang, Y.; Beames, J. M.; Lester, M. I. Velocity Map Imaging of O-Atom Products from UV Photodissociation of the CH₂OO Criegee Intermediate. *J. Chem. Phys.* **2015**, *142*, 214312.
- (16) Vansco, M. F.; Li, H.; Lester, M. I. Prompt Release of O ¹D Products upon UV Excitation of CH₂OO Criegee Intermediates. *J. Chem. Phys.* **2017**, *147*, 013907.
- (17) Moore, C. *CRC Series in Evaluated Data in Atomic Physics*; Gallagher, J. W., Ed.; CRC Press: Boca Raton, FL, **1993**, p 339.
- (18) G. Herzberg. *Molecular Spectra and Molecular Structure. III. Electronic Spectra and Electronic Strusture of Polyatomic Molecules*, 2nd ed.; Van Nostrand Reinhold: New York, 1950; Vol. 3.
- (19) Nguyen, T. L.; McCarthy, M. C.; Stanton, J. F. Relatively Selective Production of the Simplest Criegee Intermediate in a CH₄/O₂ Electric Discharge: Kinetic Analysis of a Plausible Mechanism. *J. Phys. Chem. A* **2015**, *119*, 7197–7204.
- (20) Cremer, D.; Gauss, J.; Kraka, E.; Stanton, J. F.; Bartlett, R. J. A CCSD(T) Investigation of Carbonyl Oxide and Dioxirane. Equilibrium Geometries, Dipole Moments, Infrared Spectra, Heats of Formation and Isomerization Energies. *Chem. Phys. Lett.* **1993**, *209*, 547–556.
- (21) Meng, Q.; Meyer, H.-D. A Full-Dimensional Multilayer Multiconfiguration Time-Dependent Hartree Study on the Ultraviolet Absorption Spectrum of Formaldehyde Oxide. *J. Chem. Phys.* **2014**, *141*, 124309.

- (22) Samanta, K.; Beames, J. M.; Lester, M. I.; Subotnik, J. E. Quantum Dynamical Investigation of the Simplest Criegee Intermediate CH₂OO and Its O-O Photodissociation Channels. *J. Chem. Phys.* **2014**, *141*, 134303.
- (23) Bamford, D. J.; Jusinski, L. E.; Bischel, W. K. Absolute Two-Photon Absorption and Three-Photon Ionization Cross Sections for Atomic Oxygen. *Phys. Rev. A* **1986**, *34*, 185–198.
- (24) Pratt, S. T.; Dehmer, P. M.; Dehmer, J. L. Photoionization of an Autoionizing Level of Atomic Oxygen. *Phys. Rev. A* **1991**, *43*, 282–286.
- (25) Chai, J.-D.; Head-Gordon, M. Long-Range Corrected Hybrid Density Functionals with Damped Atom–Atom Dispersion Corrections. *Phys. Chem. Chem. Phys.* **2008**, *10*, 6615–6620.
- (26) Petersson, G. A.; Bennett, A.; Tensfeldt, T. G.; Al-Laham, M. A.; Shirley, W. A.; Mantzaris, J. A Complete Basis Set Model Chemistry. I. The Total Energies of Closed-shell Atoms and Hydrides of the First-row Elements. *J. Chem. Phys.* **1988**, *89*, 2193–2218.
- (27) Petersson, G. A.; Al-Laham, M. A. A Complete Basis Set Model Chemistry. II. Open-shell Systems and the Total Energies of the First-row Atoms. *J. Chem. Phys.* **1991**, *94*, 6081–6090.
- (28) Celani, P.; Werner, H.-J. Multireference Perturbation Theory for Large Restricted and Selected Active Space Reference Wave Functions. *J. Chem. Phys.* **2000**, *112*, 5546–5557.
- (29) Shiozaki, T.; Győrffy, W.; Celani, P.; Werner, H.-J. Communication: Extended Multi-State Complete Active Space Second-Order Perturbation Theory: Energy and Nuclear Gradients. *The J. Chem. Phys.* **2011**, *135*, 081106.
- (30) Győrffy, W.; Shiozaki, T.; Knizia, G.; Werner, H.-J. Analytical Energy Gradients for Second-Order Multireference Perturbation Theory Using Density Fitting. *J. Chem. Phys.* **2013**, *138*, 104104.
- (31) Dunning, T. H. Gaussian Basis Sets for Use in Correlated Molecular Calculations. I. The Atoms Boron through Neon and Hydrogen. *J. Chem. Phys.* **1989**, *90*, 1007–1023.
- (32) Knowles, P. J.; Werner, H.-J. An Efficient Second Order MCSCF Method for Long Configuration Expansions. *Chem. Phys. Lett.* **1985**, *115*, 259–267.
- (33) Werner, H.; Knowles, P. J. A Second Order Multiconfiguration SCF Procedure with Optimum Convergence. *J. Chem. Phys.* **1985**, *82*, 5053–5063.
- (34) Hammes-Schiffer, S.; Tully, J. C. Proton Transfer in Solution: Molecular Dynamics with Quantum Transitions. *J. Chem. Phys.* **1994**, *101*, 4657–4667.
- (35) Barbatti, M.; Ruckenbauer, M.; Plasser, F.; Pittner, J.; Granucci, G.; Persico, M.; Lischka, H. Newton-X: A Surface-Hopping Program for Nonadiabatic Molecular Dynamics. *WIREs Comp. Mol. Sci.* **2014**, *4*, 26–33.
- (36) Barbatti, M.; Granucci, G.; Ruckenbauer, M.; Plasser, F.; Crespo-Otero, R.; Pittner, J.; Persico, M.; Lischka, H. *NEWTON-X: A Package for Newtonian Dynamics Close to the Crossing Seam 2018*, version 2.2; 2018.
- (37) Verlet, L. Computer "Experiments" on Classical Fluids. I. Thermodynamical Properties of Lennard-Jones Molecules. *Phys. Rev.* **1967**, *159*, 98–103.
- (38) Swope, W. C.; Andersen, H. C.; Berens, P. H.; Wilson, K. R. A Computer Simulation Method for the Calculation of Equilibrium Constants for the Formation of Physical Clusters of Molecules: Application to Small Water Clusters. *J. Chem. Phys.* **1982**, *76*, 637–649.
- (39) Butcher, J. C. A Modified MIultistep Method for the Numerical Integration of Ordinary Differential Equations. *J. Assoc. Comput. Mach.* **1965**, *12*, 124–135.
- (40) Lischka, H.; Shepard, R.; M. Pitzer, R.; Shavitt, I.; Dallos, M.; Müller, T.; G. Szalay, P.; Seth, M.; S. Kedziora, G.; Yabushita, S.; Zhang, Z. High-Level Multireference Methods in the Quantum-Chemistry Program System COLUMBUS: Analytic MR-CISD and MR-AQCC Gradients and MR-AQCC-LRT for Excited States, GUGA Spin-Orbit CI and Parallel CI Density. *Phys. Chem. Chem. Phys.* **2001**, *3*, 664–673.
- (41) Lischka, H.; Shepard, R.; Shavitt, I.; Pitzer, R. M.; Dallos, M.; Muller, T.; Szalay, P. G.; Brown, F. B.; Ahlrichs, R.; Boehm, H. J. *COLUMBUS, an Ab Initio Electronic Structure Program*; 2008.

- (42) Barbatti, M.; Granucci, G.; Persico, M.; Ruckenbauer, M.; Vazdar, M.; Eckert-Maksić, M.; Lischka, H. The On-the-Fly Surface-Hopping Program System Newton-X: Application to Ab Initio Simulation of the Nonadiabatic Photodynamics of Benchmark Systems. *J. Photochem.* Photobiol., A. 2007, 190, 228–240.
- (43) Werner, H.-J.; Knowles, P. J.; Knizia, G.; Manby, F. R.; Schütz, M.; Celani, P.; Györffy, W.; Kats, D.; Korona, T.; Lindh, R.; et al. *MOLPRO, Version 2019.1*; Cardiff, UK, 2019.
- (44) M. J. Frisch, G. W. Trucks, H. B. Schlegel, G. E. Scuseria, M. A. Robb, J. R. Cheeseman, G. Scalmani, V. Barone, G. A. Petersson, H. Nakatsuji, et al. *Gaussian 09*; Gaussian, Inc.: Wallingford, CT, 2009.
- (45) Ratliff, B. J.; Womack, C. C.; Tang, X. N.; Landau, W. M.; Butler, L. J.; Szpunar, D. E. Modeling the Rovibrationally Excited C₂H₄OH Radicals from the Photodissociation of 2-Bromoethanol at 193 nm. *J. Phys. Chem. A* **2010**, *114*, 4934–4945.
- (46) Oliver, T. A. A.; King, G. A.; Ashfold, M. N. R. Position Matters: Competing O–H and N–H Photodissociation Pathways in Hydroxy- and Methoxy-Substituted Indoles. *Phys. Chem. Chem. Phys.* **2011**, *13*, 14646–14662.
- (47) Lim, J. S.; You, H. S.; Han, S.; Kim, S. K. Photodissociation Dynamics of Ortho-Substituted Thiophenols at 243 Nm. *J. Phys. Chem. A* **2019**, *123*, 2634–2639.
- (48) Li, Y.; Gong, Q.; Yue, L.; Wang, W.; Liu, F. Photochemistry of the Simplest Criegee Intermediate, CH₂OO: Photoisomerization Channel toward Dioxirane Revealed by CASPT2 Calculations and Trajectory Surface-Hopping Dynamics. *J. Phys. Chem. Lett.* **2018**, *9*, 978–981.
- (49) Xie, W.; Domcke, W.; Farantos, S. C.; Grebenshchikov, S. Y. State-Specific Tunneling Lifetimes from Classical Trajectories: H-Atom Dissociation in Electronically Excited Pyrrole. *J. Chem. Phys.* **2016**, *144*, 104105.
- (50) Venkatesan, T. S.; Ramesh, S. G.; Lan, Z.; Domcke, W. Theoretical Analysis of Photoinduced H-Atom Elimination in Thiophenol. *J. Chem. Phys.* **2012**, *136*, 174312.
- (51) G. Ramesh, S.; Domcke, W. A Multi-Sheeted Three-Dimensional Potential-Energy Surface for the H-Atom Photodissociation of Phenol. *Faraday Discuss.* **2013**, *163*, 73–94.
- (52) Karsili, T. N. V.; Wenge, A. M.; Marchetti, B.; Ashfold, M. N. R. Symmetry Matters: Photodissociation Dynamics of Symmetrically versus Asymmetrically Substituted Phenols. *Phys. Chem. Chem. Phys.* **2013**, *16*, 588–598.

TOC Graphic

